Submerged Acoustic Retrieval

Tech 797 Final Report

Kris Hopkins, Brian Regan, Jeffrey Davies
4/25/2014

Advisor: Professor Ken Baldwin

Table of Contents:

Background:

Lobster fishing has been a key component of New England's culture and economy since early American history. It is known for its storied success with massive distribution to global fishing markets. While the beneficial impacts of this flourishing industry are quite clear, there are still major concerns being overseen. Loose fishing lines associated with lobster trap sets are proving to be costly and harmful to the surrounding eco-system. Wildlife and other boat traffic are prone to entanglement issues caused by the loose floating lines connected to the surface buoy. Most notable, the Right Whale population has suffered devastating losses due to the high fishing traffic in the Western North Atlantic. The specie's population numbers have dwindled to nearly 400 individuals in this part of the world. It is no question that the numbers will keep falling without affirmative action.

An investigation on current fishing practices around the world was necessary to determine the root causes and potential solutions to these negative ecological impacts. The issue inspired a retro-fit of the current trap system to eliminate the negative effects caused by floating lines. A new design has been modeled and analyzed that will provide alternative fishing methods while producing the same productivity and efficiency currently seen by the industry. A submersible float system was designed to eliminate the lines running from the traps to the surface buoy. The system will be incorporated into current trap designs with the use of acoustic signaling. The remote signal will provide necessary impulse to activate the release mechanism at the bottom of the ocean floor. Once released, the buoy will surface with the attached line allowing for retrieval by the deckhand. The proposed system will seamlessly integrate into current fishing practices and provide the needed ecological solution.

Abstract:

Fishing productivity with the implementation of a submerged acoustic retrieval system is critically dependent upon the surfacing buoy. MATLAB was used to provide mathematical models of each buoy's response time. Different float configurations were simulated to determine the theoretical time it would take for the system to surface from various depths. The full scale simulation was based off deepest offshore fishing occurring roughly 425 meters below the ocean's surface. After determining the theoretical surfacing time of a 14 in. trawl float was within reasonable limits, testing was performed to verify the theoretical results. The MATLAB model was modified to produce theoretical response times at a depth of 20 feet. This is the depth at which each float configuration would be tested.

The different configurations were tested against the theoretical times in the Chase Engineering Tank. This gave insight into the accuracy of the depth step model. Three different buoys were tested with multiple configurations. The surfacing times were obtained using a hand timer and a pressure sensor located at the rear of the buoy. The sensor was placed directly behind the buoy configurations to minimize its effect on the overall drag and provide greater insight into each buoy's response. The systems testing included a 9 in. lug eye buoy, an 11 in. center hole buoy, two 11 in. buoys set in parallel, two 11 in. buoys set in series, and a 14 in. center hole buoy. Both the hand time and the pressure sensor clocked the 14 in. buoy with the fastest surfacing time. It surfaced half a second faster than the next best configuration. When submerged to much greater depths, the small difference between the configuration's response times will be amplified and prove to be significant. For the same 14 in. buoy, the MATLAB analysis provided a theoretical time very close to the experimental testing time. This confirms the accuracy of the MATLAB code, meaning that accurate estimates can be made at greater working depths.

The pressure vessel housing the system's electronics was modeled in SolidWorks to understand its behavior under pressures caused by deep ocean submersions. The vessel is subject to a pressure of 445 psi at a maximum fishing depth of 425 m. To maximize durability while keeping the pressure vessel light, Aluminum Alloy 661 was chosen as the wall material. In order to fit the necessary electrical components, the inner diameter of the pressure vessel was determined to be 5.5 inches. The step was 0.1 inches and the vessel was designed with a safety factor of 1.5. The safety factor value was chosen due to the fact that the pressure at the maximum fishing depth was used during the design. The optimization tests concluded that the optimal outer diameter is 6.2 inches with a wall thickness of 0.7 inches.

The remote communication between the fishing vessel and the submerged lobster trap will be aided by the use of hydrophones. One transmitted hydrophone will be housed on the fishing vessel while the receiving hydrophone will be attached to the submerged trap. A PSOC 3 microcontroller located in the waterproof pressure vessel will process the incoming signal received hydrophone. The PSOC employs a frequency-shift key (FSK) to decompose the incoming signal into discrete frequency changes of a carrier wave. This allows for digital information to be transmitted through different codes which prevents trap theft amongst

fisherman. Once the correct signal is processed, the PSOC sends the command to open the mechanical claw through actuation of a servo motor. Due to the considerable force applied on the claw from the upward force of the buoy, two steel outriggers were attached to the arms. One element is fixed to hold the buoy when closed while the other moves on a pivot to swing out and release the buoy upon opening.

Depth Step Analysis of Surfacing Buoy

3.1- Theory of Surfacing Buoy

The response of the surfacing buoy was calculated using a depth step approach. In order to determine the surfacing time it was necessary to determine the buoy's velocity as a function of depth. Several assumptions were made to simplify the analysis. The water was assumed to have constant density and viscosity. The system is modeled for the worst case scenario, where the density and viscosity are assumed to be equal to that at 1200 feet. Secondly, the buoy is spherical and radial deflections of the buoy were considered negligible and could be ignored. This implies that the buoyant force is constant. The line attached to the buoy is considered to be neutrally buoyant which is also known as "float line."

A body rising through a fluid has multiple forces acting upon it. There is the positive buoyant force of the body (F_b). Acting against the buoyant force is the weight of the body (W), the drag of the water around the body (D_b), and the drag of the attached line (D_r). The weight and buoyant force of the buoy were provided by the buoy manufacturer. Fig.1 displays a free body diagram of the rising buoy.

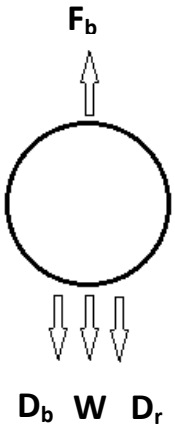

Figure 1: Sum of forces being placed on the buoy

The free body diagram shown in Fig.1 was used to produce a sum of the forces acting on the body shown in Eq.3.1

$$F = F_b - W - D_b - D_r \tag{3.1}$$

Using Newton's second law and the mass of the buoy, m, the acceleration of the buoy was determined using Eq.3.2

$$a = \frac{F_b - W - D_b - D_r}{m} \tag{3.2}$$

The depth step analysis was approached by breaking up the distance the buoy has to travel into one meter increments. The buoy was analyzed at each of these depths by recalculating the forces allowing for the determination of the terminal velocity for the preceding section. For this analysis to work, it was first assumed that the acceleration of the rising buoy was zero. In reality the acceleration will be slightly negative as the buoy slows with an increase in rope drag, however the acceleration change over the set distance is so small it can be neglected.

Using zero acceleration in Eq. 2 allows for simplification which results in Eq.3.3

$$F_b - W = D_b + D_r \tag{3.3}$$

The drag of the rope D_r can be modeled by the following equation.

$$D_r = \frac{1}{2} * \rho * V^2 * S_r(L) * C_{dr} \tag{3.4}$$

Where ρ represents the density of seawater, V represents the velocity of the body, $S_r(L)$ represents the surface area of the rope as a function of rope length L, and C_{dr} represents the coefficient of drag of the rope which was given in the rope manufacturer's specifications.

The surface area of the rope as a function of rope length $S_r(L)$ was calculated using the rope's radius r_r and the following equation.

$$S_r(L) = 2\pi r_r L \tag{3.5}$$

The drag of the buoy D_b can be modeled by the following equation.

$$D_b = \frac{1}{2} * \rho * V^2 * A_b * C_{db} \tag{3.6}$$

Where C_{db} is the coefficient of drag of the sphere and A_b represents the effective area of the sphere. Using the sphere's radius r_b, the effective area A_b was calculated using the following expression.

$$A_b = \pi {r_b}^2 \tag{3.7}$$

The equation for determining the Reynolds number of a sphere traveling through a fluid is shown in Eq.3.8

$$Re = \frac{\rho V_{est} D}{\mu} \tag{3.8}$$

where D is the diameter of the buoy and μ is the dynamic viscosity of seawater. A range of buoy velocity estimates V_{est} were used to calculate an array of Reynolds numbers. The resulting values were analyzed and used to provide an estimate of the coefficient of drag of the sphere C_{db}.

Substituting Eq.3.4 and Eq.3.6 into Eq.3.3 produced the following result.

$$F_b - W = \left(\frac{1}{2} * \rho * V^2 * S_r(L) * C_{dr}\right) + (\frac{1}{2} * \rho * V^2 * A_b * C_{db}) \tag{3.9}$$

Simplifying Eq.3.9 to solve for the velocity of the body as a function of rope length $V(L)$ produced the following equation.

$$V(L) = \sqrt{\frac{2(F_b - W)}{\rho[(S_r(L) * C_{dr}) + (A_b * C_{db})]}} \tag{3.10}$$

Eq.3.10 provided the average velocity of the body for the previously stated 1 meter depths increments. Knowing distance traveled and speed of the buoy made it possible to determine the time elapsed during each depth interval. This is shown by the following equation.

$$time = \frac{d}{V} \tag{3.11}$$

Where d is the depth interval used in the depth step analysis. With the elapsed time at each step known, it was possible to sum the time intervals to determine the total time required for the buoy to surface. The total surfacing times were then plotted with respect to rope length to provide a visual aid in understanding the problem.

3.2- Determination of the Coefficient of Drag of the Surfacing Buoy

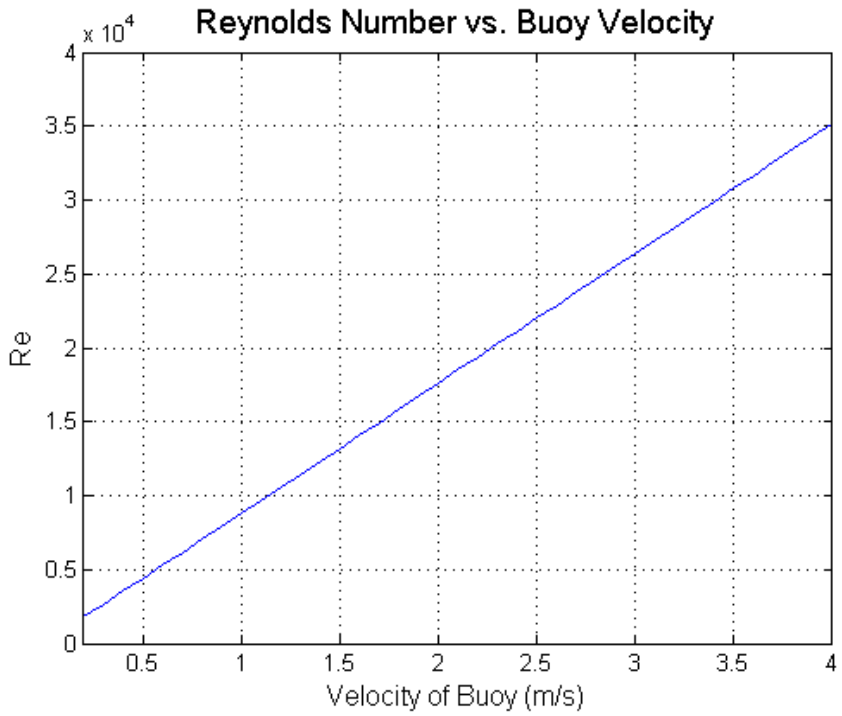

Figure 3: Graphical representation of the Reynolds number vs. velocity of the buoy

The Reynolds number was estimated with a range of buoy velocities from 0.2 m/s to 3 m/s. As shown in Fig.3, the resulting Reynolds numbers ranged from $1.8*10^3$ to $3.5*10^4$.

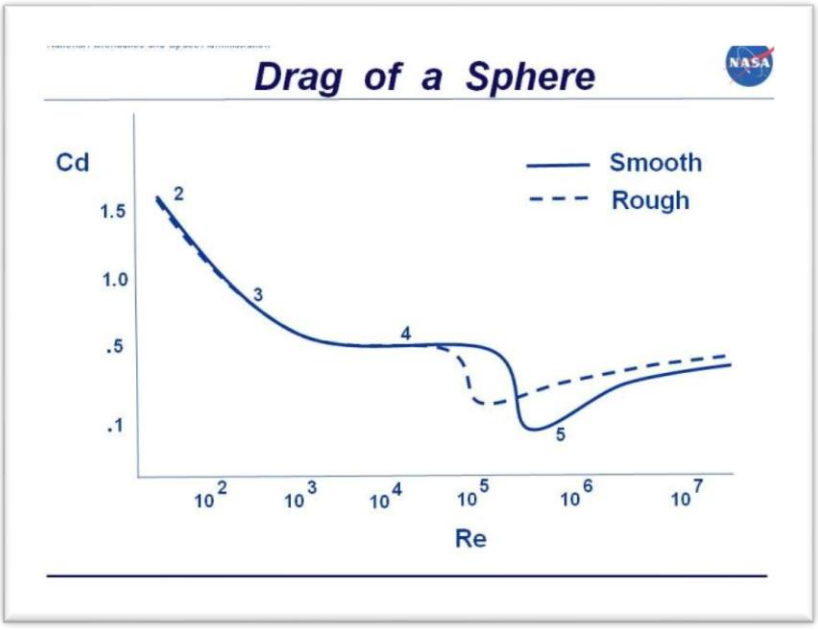

Figure 4: Relationship between the coefficient of drag of a sphere and the Reynolds number

Fig.4 shows the coefficient of drag of a sphere with respect to Reynolds number. The range of estimated Reynolds numbers shown in Fig.3 all fell within the flat section of the smooth drag curve represented by the number 4. Due to the consistency of the coefficient of drag throughout the broad range of velocities it was safe to assume a constant drag coefficient of 0.47.

3.3- Theoretical Time Responses of Surfacing Buoy Systems

The surfacing time response of each buoy configuration was modeled in MATLAB for submersion depths up to 6 meters. The UNH Ocean Engineering Tank provided an experimental testing depth of 20 feet (roughly 6 meters). The theoretical and experimental times were compared to verify the accuracy of each configuration's mathematical model.

Figure 5: Time response of the 9" lug eye trawl float

Fig.5 shows the theoretical surfacing time response of the 9 inch trawl float with lug eyes. The estimated time for the buoy to travel 6 meters was 4.99 seconds.

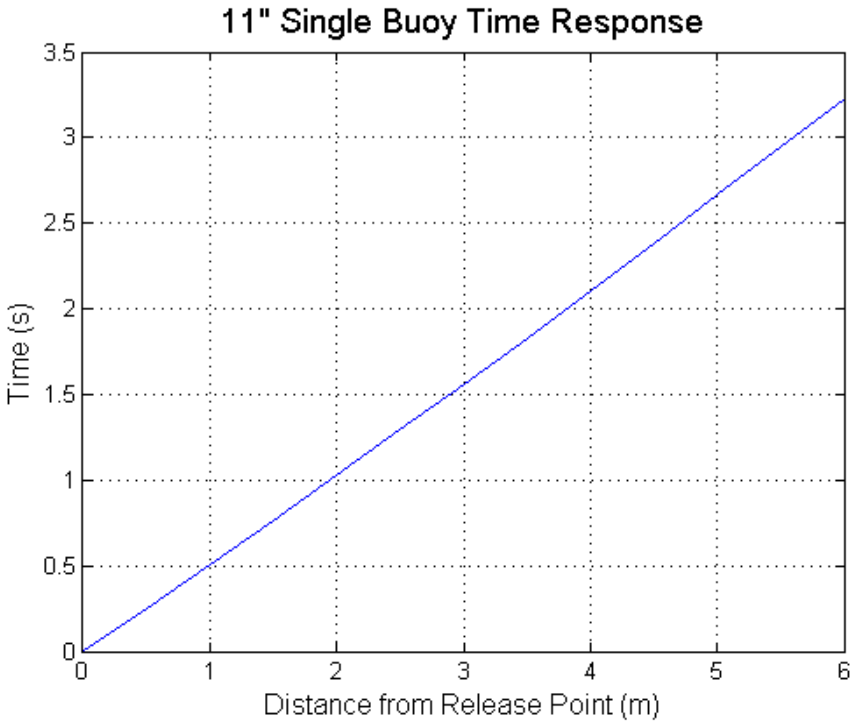

Figure 6: Time response of the 11" center hole trawl float

Fig.6 shows the theoretical surfacing time response of the single 11 inch trawl float. The estimated time for the buoy to travel 6 meters was 3.21 seconds.

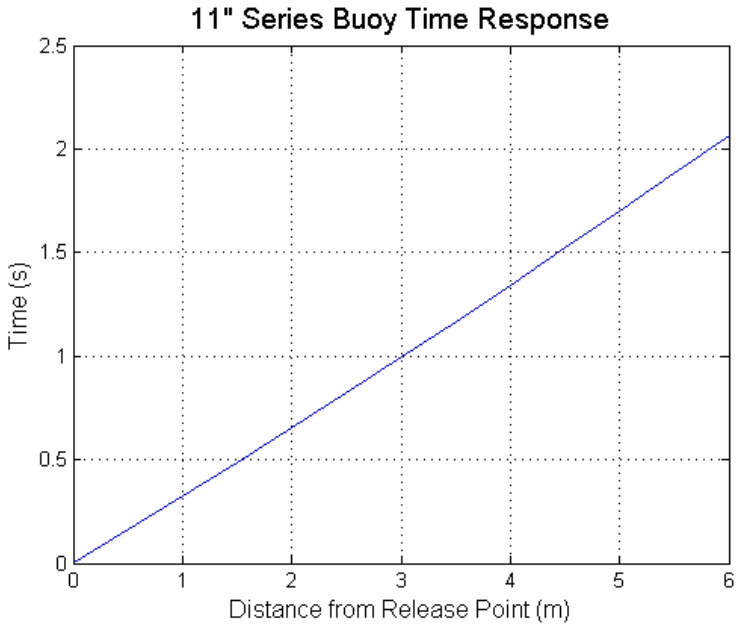

Figure 7: Time response of the 11" series configuration

Fig.7 shows the theoretical surfacing time response of the two 11 inch trawl floats placed in series. The estimated time for the system to travel 6 meters was 2.05 seconds.

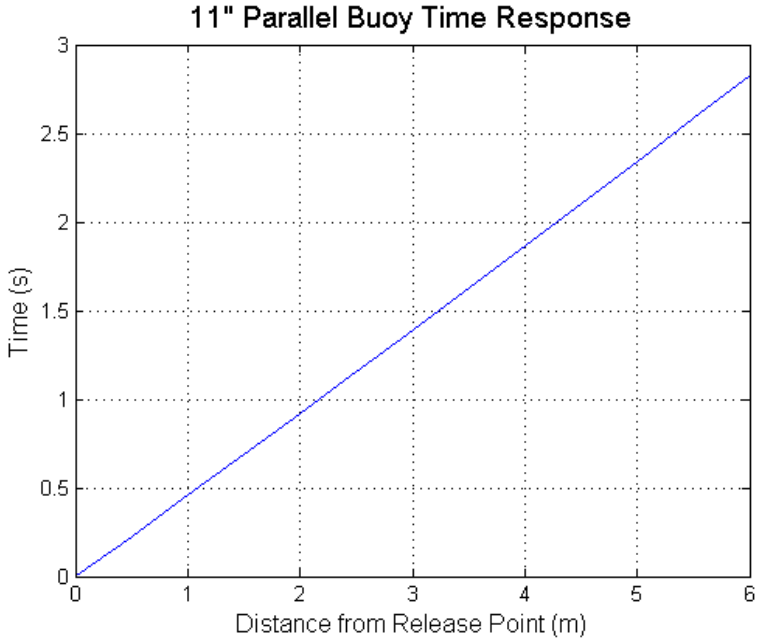

Figure 8: Time Response of the 11" parallel configuration

Fig.8 shows the theoretical surfacing time response of the two 11 inch trawl floats placed in parallel. The estimated time for the system to travel 6 meters was 2.82 seconds.

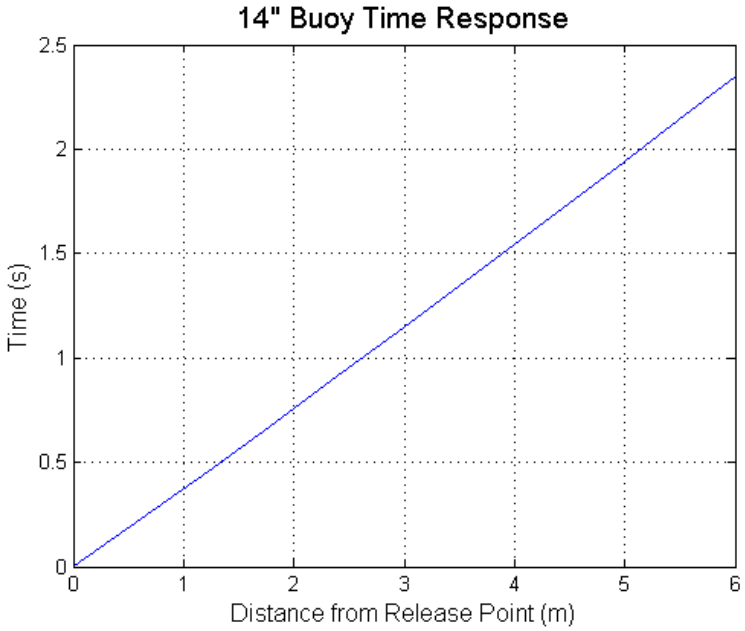

Figure 9: Time Response of the 14" trawl float

Fig.9 shows the theoretical surfacing time response of the 14 inch center hole trawl float. The estimated time for the system to travel 6 meters was 2.34 seconds.

3.4- Verification of the Buoy's Coefficient of Drag

Float Type	Minimum Velocity (m/s)	Maximum Velocity (m/s)
9" Lug Eye	0.2250	1.3110
Single 11"	0.4130	1.9835
Two 11" in Series	0.6468	3.1064
Two 11" in Parallel	0.6332	2.1966
Single 14"	0.6962	2.6622

Table 1: Velocities corresponding to float size

Table 1 shows the resulting velocities from the theoretical time response models. The minimum and maximum velocities of each float system were recorded to back check the previous estimates made on the surfacing velocity. The coefficient of drag for the spheres only held true if the surfacing velocity stayed within the estimate bounds of 0.2 m/s to 4 m/s. As shown by Table 1, all minimum and maximum velocities fell within the estimation range. This indicates the use of 0.47 as the sphere's coefficient of drag was appropriate.

3.5- Experimental Time Responses of Surfacing Buoy Systems

	Surfacing Time from 6 Meter Depth		
Float Type	**Theoretical (s)**	**Avg. Experimental (s)**	**% Error**
9" Lug Eye	4.99	3.82	30.63 %
Single 11"	3.21	2.65	21.13 %
Two 11" in Series	2.05	2.74	25.18 %
Two 11" in Parallel	2.82	4.31	34.57 %
Single 14"	2.34	2.25	4.0%

Table 2: Surfacing time by float size

Table 2 shows the theoretical and experimental surfacing times of each float system from a depth of 6 meters. The theoretical analysis produced an estimation that the two 11 inch buoys set in series would produce the fastest surfacing time at 2.05 seconds. The slowest theoretical response was expected to be seen by the 9 inch trawl float with lug eyes at 4.99 seconds. The experimental results showed the fastest response time was achieved by the single 14 inch trawl float. This clocked in at an average of 2.25 seconds. The slowest recorded experimental setup was seen by the two 11 inch buoys set in parallel with an average time of 4.31 seconds. The largest percent error was produced by the theoretical and experimental comparison of the two

11 inch buoys in parallel. The percent error for this system was 34.57%. The smallest percent error was achieved by the single 14 inch trawl float. This system produced a percent error of 4.0%. The remaining surfacing systems had high percent errors ranging from 21.12%-30.63%.

Pressure Vessel Analysis:

4.1 - Pressure Vessel Introduction

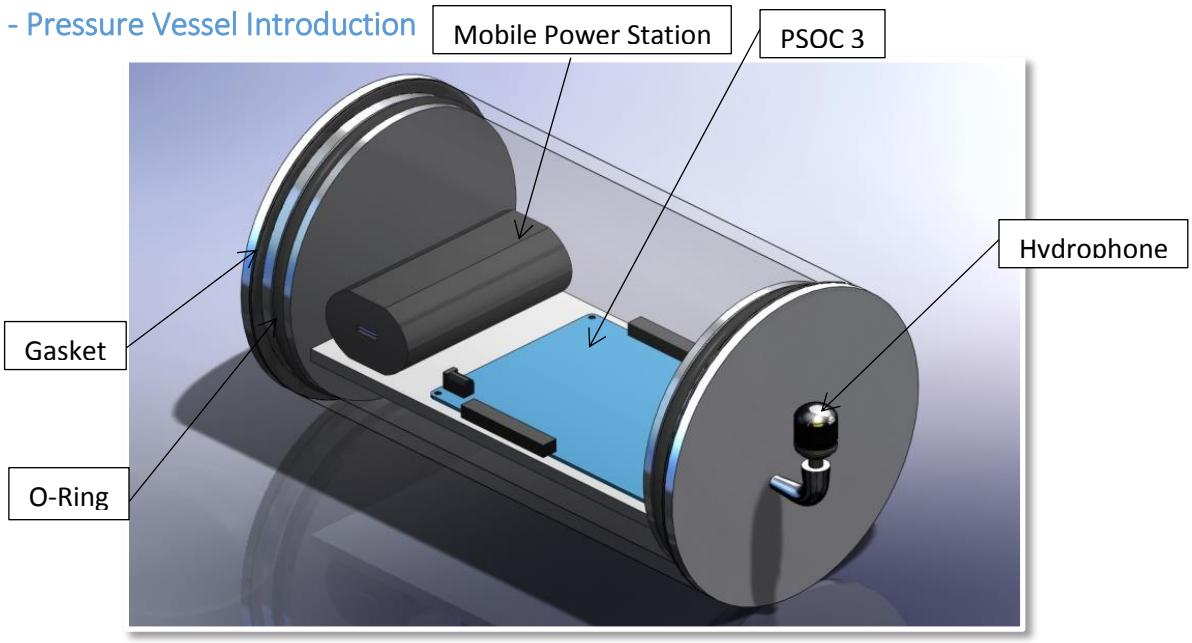

Figure 10: Pressure vessel component design

Electrical component storage is vital when it comes to the functionality of a submerged acoustic retrieval system. For the electrical components to stay water free a pressure vessel was designed using the 3-D modeling software Solidworks. The pressure vessel was designed to house the cypress PSOC 3 microcontroller and GearPower ultra capacity mobile power station. In order to fit the PSOC and power station the inner diameter of the pressure vessel was determined to be 5.5 inches. With inner diameter determined the rest of the pressure vessel could be designed. To keep the vessel water tight an O-ring and Gasket are used on each end cap as can be seen in Figure 10. Each end cap of the pressure vessel will be secured using two pressure clamps. The pressure clamps allow for reasonable end cap removal for power stations changes. One end cap is designed with two through-wall taps, used to run wires to the servo and hydrophone.

When designing the pressure vessel the highest pressures the vessel will face needed to be taken into account. Currently offshore lobster fishermen fish the deepest at a depth of 1000ft. The pressure at 1000 ft corresponds to a pressure that is approximately 445 psi. Using the pressure of 445 psi an optimization study was performed using the Finite Element Analysis (FEA) package in Solidworks. The goal of the optimization study was to determine the optimal

wall thickness of the pressure vessel. The material used for the analysis was 6061 aluminum. Aluminum was used due to its resistance to salt water corrosion as well as the relatively cheap cost.

4.2 - Optimization Study

The optimization study solely focused on the cylindrical wall thickness due to the max stress occurring on the inner wall of the cylinder.

Design Variables

Name	Type	Values	Units
Outter Diameter	**Range with Step**	Min:5.5 Max:6.5 Step:0.1	in

Constraints

Sensor name	Condition	Bounds	Units	Study name
Stress1	**is greater than**	Min:1.500000	FOS	Pressure Study

Goals

Name	Goal	Properties	Weight	Study name
Mass1	Minimize	Mass	10	Pressure Study

Figure 11: Table of initial parameters set for optimization study

The factor of safety was used as the constraint with a minimum value of 1.5. The factor of safety was chosen because the pressure that is being used in the analysis is the absolute maximum pressure the vessel will see therefore the factory of safety does not need to be large. The goal of the optimization was to keep the weight as minimal as possible.

The optimization successfully ran and the optimal wall thickness was determined to be .35 inches. The study showed the optimal condition to be an outer diameter of 6.2 inches and with an inner diameter of 5.5 inches this resulted in the wall thickness of .35 inches.

Component name	Units	Current	Initial	Optimal	Scenario1	Scenario2
Outer Diameter	in	6	6	6.2	5.5	5.6
Mass1						
Stress1	lb	1.2653810.821422	1.265380.8214221	1.5018730.994505	--	0.3409830.49228

Component name	Units	Scenario3	Scenario4	Scenario5	Scenario6	Scenario7
Outter Diameter	in	5.7	5.8	5.9	6	6.1
Stress1		0.683440	0.822909	1.167482	1.265381	1.406880
Mass1	lb	0.572437	0.654013	0.737008	0.821422	0.907254

Component name	Units	Scenario8	Scenario9	Scenario10	Scenario11	<L_Iter5/>
Outter Diameter	in	6.2	6.3	6.4	6.5	<SR_Iter5/>
Stress1		1.501873	1.540014	1.629830	1.712806	
Mass1	lb	0.994505	1.08317	1.17326	1.26477	

Figure 12: Results of optimization study

4.3 - Theory of Optimization:

The area which was most likely to fail under the given pressures was the cylindrical walls of the capsule. To evaluate the loads in these walls equations 4.1, 4.2 and 4.3 were used in conjunction with the dimensions from the optimized model. First the capsule was checked for buckling using equation 4.1. Since the walls of the capsule are thicker than the calculated t_{crit} value, the capsule won't buckle under the given load.

$$t_{crit} = \frac{d}{2}\left(1 - \sqrt{\frac{2P}{\sigma_{yield}}}\right) = 0.1848\ inches \tag{4.1}$$

The longitudinal and hoop stress of the walls were also checked using equations 4.2 and 4.3. The hoop stress was the larger of these two stresses. Since the pressure was external, cylinder is in compression, as opposed to tension which typically occurs with internal pressure. The hand calculated hoop stress matched well with the Von Mises stress found in Solidworks.

$$\sigma_{long} = \frac{Pr}{2t} = 1851.25\ psi \tag{4.2}$$

$$\sigma_{hoop} = \frac{Pr}{t} = 3702.5\ psi \tag{4.3}$$

4.4 – Analysis of Optimization

Due to symmetry the model which was used in the simulations, shown in figure 12 below, was one quarter of the total model. In order to account for this symmetry constraints were used on all the faces which were cut. To simulate the bottom of the capsule being fixed to a trap, a fixed constraint was used on the base of the capsule; all the applied constraints are shown in figure 12 as green arrows. A pressure loading of 14.7 psi was applied to all the internal surfaces of the capsule to simulate the internal pressure. To simulate the external pressure a 445psi pressure

load was applied to all the external surfaces of the capsule, all the applied loads are shown in figure 12 as red arrows.

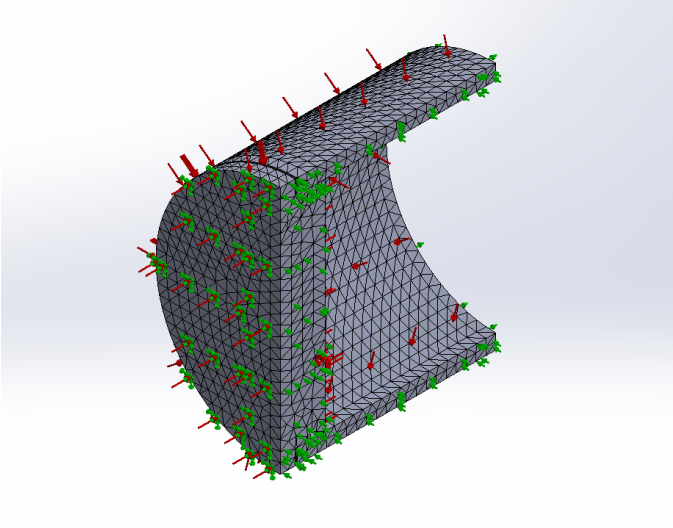

Figure 13: Model showing constraints, loading conditions and converged mesh of .25" mesh size

A convergence test was run on the optimized model using the 2nd principal stress in order to find the mesh size at which the mesh converged. The results are plotted in figure 13. The mesh size found from the convergence study and used for the analysis was .25".

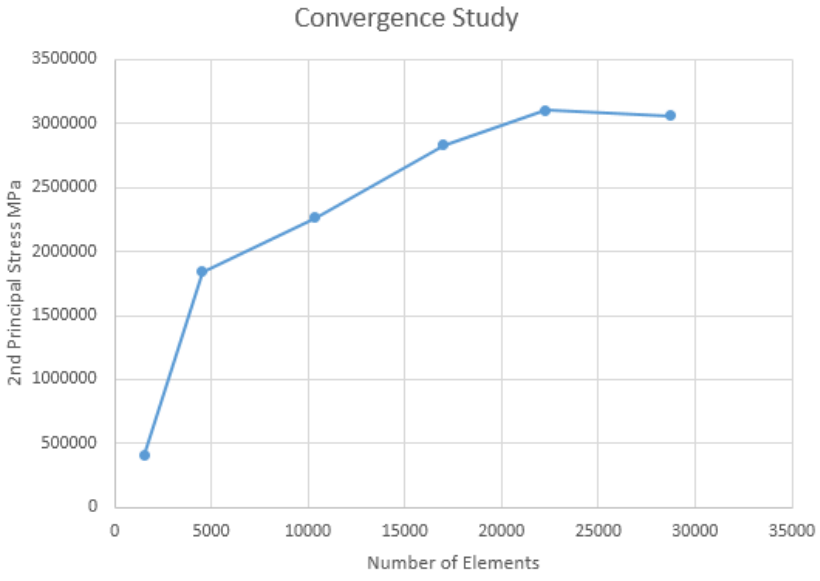

Figure 13: Results from convergence study on the optimized model

The resulting stress for the simulation described above is shown in figure 14. The highest stress can be seen on the inside of the cylindrical face with a maximum Von-Mises stress

The resulting displacements from the pressure analysis are shown in figure 15. The highest displacements are in the cylindrical walls of the pressure vessel with a maximum displacement of .025mm or $9.85x10^{-4}$ in, these displacements were determined acceptable to maintain the function of the capsule.

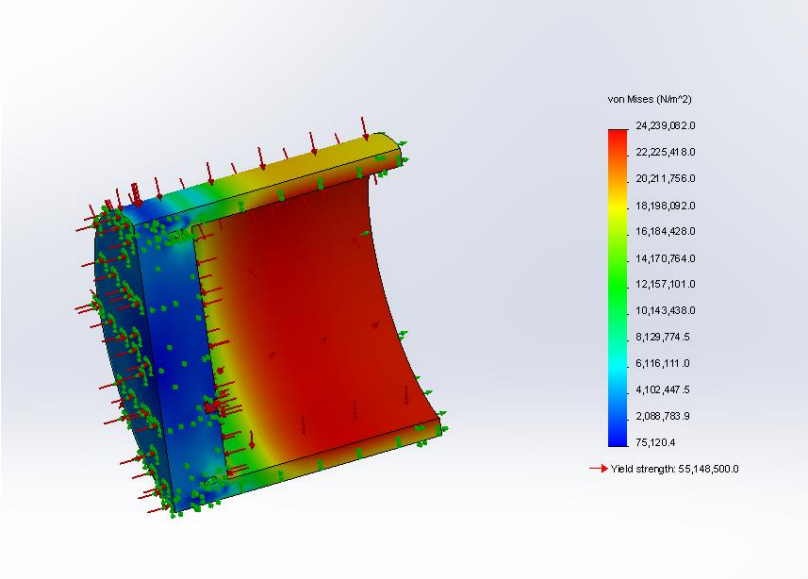

Figure 14: Von Mises stress results from pressure analysis on the optimized model

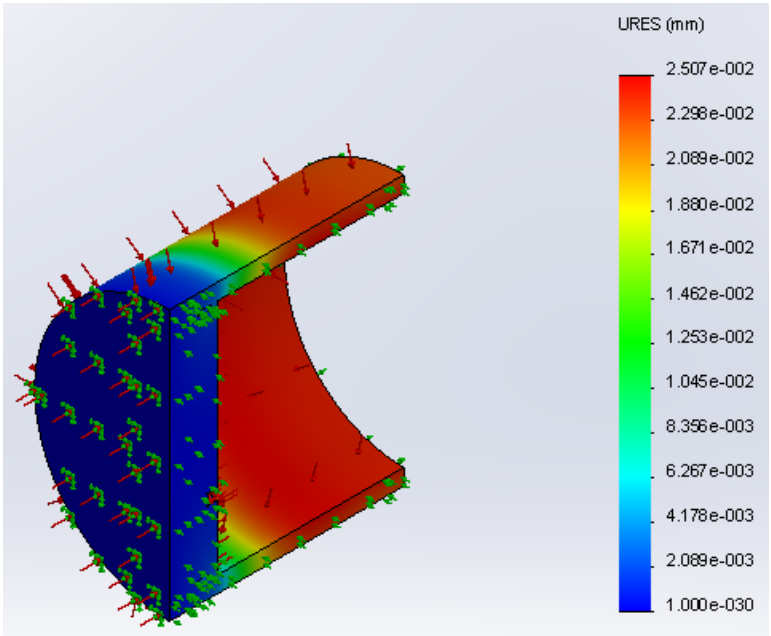

Figure 15: URES displacement results from pressure analysis on the optimized model

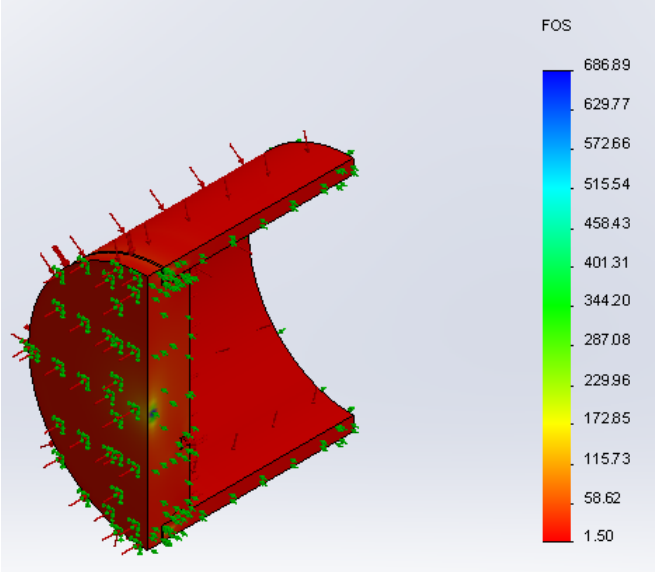

Figure 16: Factor of Safety plot using Von Mises stress results on the optimized model

The factor of safety plot which was determined using the von Mises stress is shown in Figure 16. The minimum factor of safety is located on the cylindrical walls and the highest factor of safety was located in the base of the capsule. This indicates that the area's most likely to fail are the walls of the capsule.

4.5 – Optimization Conclusion

Solidworks was used to design and test a pressure vessel that will be used for storing electrical components needed for the Rope Less Fishing mechanical release. The pressure vessel was made to be a cylinder with at ends. An initial stress test was conducted using the pressure found at 1000 feet below sea level which amounts to 445 psi. With the initial design complete, an optimization study was used to determine the cylinder thickness with the constraint of a minimum factor of safety of 1.5. The optimal size of the cylinder was determined to be and inner diameter of 5.5 and an outer diameter of 6.2 which was rounded up to have a thickness of .375. The model was then tested for a mesh convergence and the max stress was determined. Hand calculations were done and compared to the simulation output with similar results. Buckling calculations were as well performed and resulted in no buckling.

Electronic Components:

5.1 – Signal Processing

For the mechanical release to work there needs to be communication between the boat and trap. Communication between the boat and trap is conducted through the use of sonar technology. The sonar technology needed for communication is similar to what can be found on most fish finders. The fish finders send frequency signals at either 50 or 200 kilo hertz that travel through the water and return the

location of fish. In a similar manner to the fish finders, a frequency signal with be transmitted from the boat and received by the trap along the ocean floor thus releasing the buoy for trap retrieval. Originally the goal was to use a 50 kHz signal to trigger the release. It was then determined that a single frequency would not be all that was needed.

One of the main goals of the acoustic release system is to reduce the amount of traps lost due to whale and boat entanglement. If a single frequency was used the traps could easily succumb to theft with someone simply sending out the same frequency and triggering the mechanical release. To avoid theft and other possible modes of release a digitized code was thought up as a way to avoid such issues. How the digitized code works is along the same lines as a telephone number. The code would consist of a 5 to 8 digit code which consists of ones and zeros with both the one and zero representing a different frequency. For example a 49 kHz signal would represent a zero and a 51 kHz signal would represent a one. The frequencies would then be dialed just as a telephone call would. Once the trap has received the correct code only then will the release open and the buoy sent to the surface.

5.2 – Hydrophones

To solve the problem of communication it was determined that hydrophones would be the best transducers. Hydrophones are fairly low cost, durable and low maintenance which are very beneficial to the lobster industry. The hydrophones used for the proof of concept design were purchased from Aquarian Audio Products. The specific hydrophones used are the H1c and H1a with the difference being a BNC connector on the H1a. The hydrophones were fairly inexpensive each with a cost of approximately $130 U.S. Unfortunately because the hydrophones were cheap they were also not calibrated and had a smaller usable frequency range. A more expensive hydrophone such as one from Teledyne Benthos would have larger frequency range. Due to the small frequency range of the hydrophones purchase the proof of concept could not use the common 50 kHz frequency. It was instead determined that the frequencies used would be within the audible range, less than 10 kHz. For a commercial acoustic release a hydrophone with a greater frequency range would be implemented.

5.3 – Microprocessors

The microprocessor is an essential component in the design of the acoustic release. The microprocessor is responsible for processing the signals received by the hydrophone and activating the release. For the proof of concept design two microprocessors were used one for transmission and the other for receiving. The microprocessors used for proof of concept are Cypress PSOC 3 developer boards. The boards cost approximately $110 each. A Cypress representative aided in the proof of concept design.

For proof of concept it was determined that frequency hopping would not be needed and instead Frequency Shift Keying (FSK) was to be used. FSK is the altering of two frequencies to deliver data. Just as with the frequency hopping there are two frequencies each representing either a 0 or 1. The frequencies alter back and forth at a pre-determined time step. The frequencies used for proof of concept were 2100 Hz and 1300 Hz due to the hydrophone restrictions. On the receiving end the incoming signal needed conditioning to enable the PSOC to trigger the release. The incoming signal from the hydrophone was sent through a circuit to condition the signal to have a center frequency of 1500 Hz and a band width of 1570 Hz. The signal was then sent through a band pass filter to try to remove ambient noise. Once the signal as be processed by the band pass filter the frequency shift keying is analyzed. On recognition of the set pattern the servo will open the claw.

For the proof of concept there were however some issues when using the PSOC microprocessors. The PSOC, just like the hydrophone, is limited to a lower frequency due to the sampling rate the PSOC can achieve. It was determined that the maximum frequency input could only be around 30 kHz due to the sampling rate needed to be around 3 times the sampled frequency. Higher frequencies that are needed for commercial operation will require a more powerful processor.

The proof of concept as well ran into issues when attempting to communicate between the two hydrophones. The hydrophones were tested by attaching one to the function generator and the other to the oscilloscope. Initially the signal was not showing on the receiving side. It was realized that a significant amount of amplification was needed in order for the signal to be identified. A 12v high pass amplifier was attached to the output hydrophone. The addition of the amplifier made the signal clearly visible when the Fast Fourier Transform was viewed. Unfortunately when using the microcontrollers the test was not very successful. It was clearly evident that the transmission hydrophone was functioning properly due to the audible tones coming from the hydrophone. The receive side did not fare so well during the testing. The receive side was not showing the incoming signal and did not trigger the servo.

As with the original test the thought is that the amplification used by the receiving microprocessor is not enough. The goal for the upcoming couple of weeks is to finalize the set up and have the hydrophones functioning properly. It is very feasible that the hydrophones will work with just a simple code tweak and added amplification.

Mechanical Release:

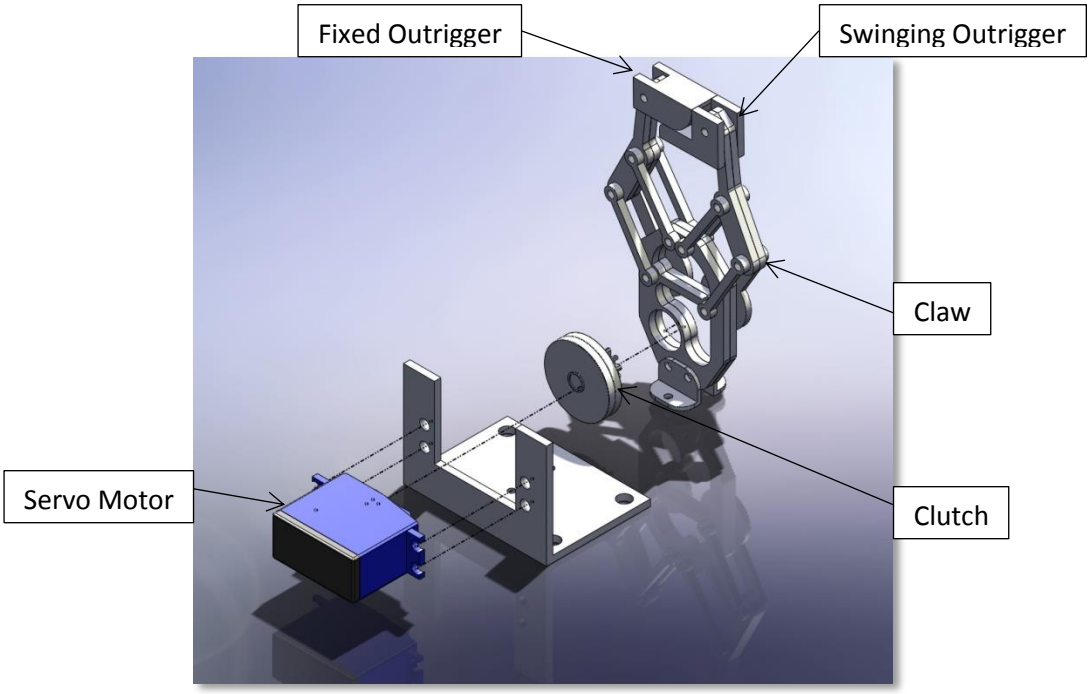

Figure 17: Proof of concept mechanical release design

6.1 – Servo Motor

Upon receiving the correct coded signal from the transmitting hydrophone, the receiving microcontroller will signal the servo motor to actuate. The servo motor used for proof of concept is a Traxxas 2056 high-torque waterproof servo motor. The waterproofing allows for full water submersion outside of the waterproof pressure vessel. The servo motor has waterproof wires running from the motor to the PSOC 3 microcontroller housed in the pressure vessel. The pressure vessel stays air-tight with a waterproof wire through-pass that allows the internal wires to run out to the mechanical components.

6.2 – Release Claw

The mechanical gear of the servo is connected directly to the gears of the mechanical release claw. When the servo is commanded to actuate open, the mechanical claw's gears will rotate and open the catch mechanism. The mechanical release is a small scale aluminum claw with several custom modifications. Two aluminum outriggers were added the claw to reinforce the catch mechanism that experiences large buoyant forces exerted by the buoy. One of the outriggers is fixed to safely hold the buoy clip when closed. The other outrigger is fixed on a

pivot point which allows the arm to swing freely when the claw is in the open position. The swing allows for the buoy clip to release from the trap system and float to the surface.

Conclusions

The objective for this experiment was to design a lobster fishing system incorporating a submerged acoustic retrieval that easily integrates into current fishing practices. The first step in determining the feasibility of the project was to determine the surfacing times of submerged buoys. This analysis included a theoretical MATLAB simulation and experimental testing in the Chase Ocean Engineering tank. The results were used to test if the buoys could surface fast enough for fishing implementation, and if they did, to see which buoy surfaced the fastest. The theoretical and experimental results were then compared to determine the accuracy of the model. The accuracy of the model would indicate whether or not an analysis could be performed at any potential fishing depth.

The theoretical surfacing model was created with the initial assumption that the Reynolds number of the buoy stayed within 10^3 and 10^5. This range corresponds to a coefficient of drag of 0.47. After the model was run for each buoy configuration, the surfacing velocity at each point of the surfacing was verified. In order for the initial assumptions to be accurate, the buoy velocities had to stay within a range of 0.2 m/s to 4 m/s. Every buoy was confirmed to be within this range, confirming that the buoy's drag coefficient estimate of 0.47 was accurate.

The pressure sensor located at the rear of the buoys was used for additional data that could be compared to the hand times taken with a stopwatch. The pressure sensor device was limited to recording one data point per second. The one second interval did not provide enough accuracy when timing the quick buoy responses so the pressure data was ignored. The multiple trials recorded by hand produced a small standard deviation so it was determined that the best experimental time could be produced by taking an average of the multiple test times.

From the testing it was found that the fastest surfacing time corresponded to the 14 inch trawl float with a time of 2.25 seconds. This was then compared to the theoretical time of 2.34 seconds to yield a percent error of 4.0%. Not only was this the fastest surfacing time, but it was also the smallest percent error. Looking at the results for the other buoys, a trend from the data was noticed. The faster the experimental surfacing times, the smaller the percent error. This trend could be due to the fact that the faster times corresponded to larger buoys, and the larger buoys could have created a wake big enough to minimize the effects of drag from the pressure sensor located at the rear of each buoy. Aside from the 14 inch buoy, the other buoys had much higher percent errors ranging from 21.12%-34.57%. These large errors are also due

to the complications that came with modeling the buoys in MATLAB. The non-uniform shapes of the multiple buoy configurations made it difficult to appropriately simulate the drag effects in the mathematical model. Combined with the unsteady surfacing of the combination floats, a large percent error was likely to occur.

The 14 inch buoy was selected due to the quick surfacing time and the accurate mathematical model developed in MATLAB. The accuracy of the model indicates that a precise estimate can be made for deeper submersion scenarios. Modeled at depths of 425 meters, which is the greatest working depth for offshore fishing, a time of 7.1 minutes was found. This time is fast enough to not limit work productivity and therefore will not hinder current fishing practices.

The remote communication between the fishing vessel and the submerged trap required the use of two acoustic hydrophones. The boat houses a hydrophone that transmits alternating carrier waves at two different frequencies that correspond to either a 0 or a 1. A unique alternation between the 0 and 1 frequency provide ships with a code that can be used to communicate with their trawl sets and prevent theft from other fishing operations. The receiving hydrophone submerged with the auxiliary trap will intercept the ship's signal only if it corresponds to the correct pre-programmed code. Once the hydrophone receives the correct signal, a PSOC 3 microcontroller connected to the hydrophone will command the servo motor to actuate and open the mechanical claw, thus sending the buoy off to the surface.

The hydrophone will connect to the PSOC 3 through a wire-tap running into the waterproof pressure vessel. The waterproof vessel was designed to house the PSOC 3 and the battery pack used to power the microcontroller. The finite element analysis package of SolidWorks was used to determine the optimum design that would withstand the pressure associated with deep ocean submersion. The pressure vessel was designed with an outer diameter of 6.2 in. with a wall thickness of 0.7 in. This minimal design has a small cost and size impact when incorporating it into the auxiliary trap.

Our analysis confirmed the potential use of a submerged acoustic retrieval system integrated into current fishing practices. The environmental benefits seen form such operations far outweigh the minimal economic impact seen by fisherman. The new system will rid the ocean of cluttered fishing gear and free up fishing lanes and marine animal migration routes. The North Atlantic Right Whale population will be free to regain strength and maintain the balance of a delicate ecosystem.

Project Future

In the coming years, it is our goal to have this project continued by future students in the Tech 797 class. The analysis and experimental testing completed this year have laid a good foundation to build upon. Currently, the most difficult part of the project is transmitting and receiving a signal with the hydrophones. To accomplish this communication a larger budget will be necessary. The hydrophones currently used, purchased from Aquarian Audio, operate at such a small frequency that they can only communicate from a close distance. To successfully implement this design across the fishing industry, communication is going to have to happen from up to 425 m apart. Hydrophones of this quality can cost anywhere from $1,000 to $3,000. With a larger budget this can be feasible. This does, however, create a problem with the implementation. The goal of this project is to seamlessly integrate into current fishing practices and with a high price for the whole system this will be a much harder task. The price can be reduced through multiple avenues. On a mass production scale, the price for all components will be decreased, but it will still be an expensive transition. The other major factor that will affect this price is due to the declining population of North Atlantic Right Whales. With their rapid decline in numbers, government intervention is only a few year down the road. This intervention will hopefully come with grants and subsidies to the local fishing businesses that can make the system affordable.

A major problem that the design faces is through mechanical malfunctions while at the bottom of the ocean. While these malfunctions are not expected to happen frequently, it is an inevitable consequence of using technology of this kind. If the buoy does not float to the surface and there is no fail-safe, thousands of dollars of equipment could be lost. One possible solution for this problem is to install a corrodible pin in the mechanical release. This pin would corrode if left in the water for a longer period of time than usual and the buoy would be released to the surface. This would save the traps from being lost and they could be retrieved at a later juncture.

Building upon our project, improvements could be made and components upgraded. The concept for the trap system works and has been shown valid through the proof of concept analysis. However, the mechanical release needs to be made larger and more durable. For our experimental testing, the robotic claw functioned perfectly, but it would not be able to withstand the upward force from a 14 in. buoy. Possible suggestions include making a larger more durable claw, with the same updated outriggers, or designing a new mechanical release completely. With these suggestions, the current Submerged Acoustic Retrieval team hopes that moving forward the project will see unparalleled success.

Appendix

8.1 – Figures

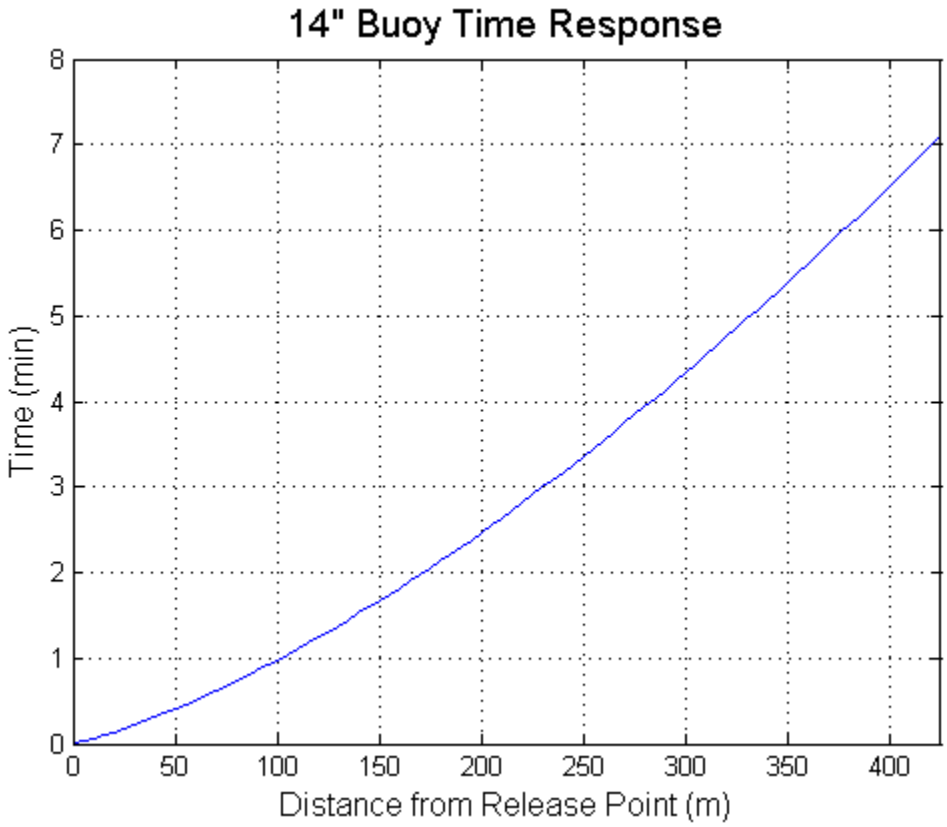

Figure 8.1: Time response of the 14 inch buoy at submersion depths up to 425 meters

8.2 - Data Tables

9" Lug Eye	
Test #	*Hand Time*
1	*3.7*
2	*3.91*
3	*3.86*
Average	*3.82*

Table 8.1: Hand time results for 9" buoy

11" Center Hole	
Test #	*Hand Time*
1	*2.9*
2	*2.53*
3	*2.6*
4	*2.55*
Average	*2.65*

Table 8.2: Hand time results for single 11" buoy

2 X 11" Center Hole (Parallel)	
Test #	*Hand Time*
1	*4.21*
2	*4.4*
Average	*4.31*

Table 8.3: Hand time results for two 11" buoys in parallel

2 X 11" Center Hole (Series)	
Test #	*Hand Time*
1	*2.57*
2	*2.9*
Average	*2.74*

Table 8.4: Hand time results for two 11" buoys in series

14" Center Hole	
Test #	*Hand Time*
1	*2.65*
2	*2.05*
3	*2.18*
4	*2.1*
Average	*2.25*

Table 8.5: Hand time results for single 14" buoy

8.3 - MATLAB Code

```
clc
clear all
close all

% Environment Specs
row=1025.7; %density of seawater kg/m^3
%row=998.19; %density of freshwater kg/m^3
u=1.08*10^-3; %dynamic viscosity kg/m*s
v=1.609*10^-6; %kinematic viscosity m^2/2
g=9.807; %gravity m/s^2
radr=0.009525/2; %radius of hydropro rope in m

% 9 in Lugeye Bouy Specs
%radb=0.2286/2; %radius of buouy m
%vol=(4/3)*pi*(radb^3); %volume of buouy m^2
%W=22.596965871509997; %buouy weight in N
%B=39.1443503286; % Bouyancy in N

% 11 in Bouy Specs
%radb=0.2794/2; %radius of buouy m
%vol=(4/3)*pi*(radb^3); %volume of buouy m^2
%W=25.62175657872; %buouy weight in N
%B=82.20313569006; % Bouyancy in N

% 14 in Bouy Specs
radb=0.3556/2; %radius of buouy m
vol=(4/3)*pi*(radb^3); %volume of buouy m^2
W=69.92604399609/g; %buouy weight in N
B=172.23514144584; % Bouyancy in N

% Depth (m)
x=1;
L=0:x:425;

% Reynolds number with estimated velocity
Vest=.2:.1:4;
Re=(row*radr*2/u).*Vest;

Cdr=.05; % Hydropro rope, manufacturer's specs
Cdb=.47; % Based off Reynolds number (laminar flow)

% Effective Areas
Ar=(2*pi*radr).*L;
Ab=pi*(radb^2);

% Find velocity
V=sqrt((B-W)./((.5*row)*(Ab*Cdb+Ar*Cdr)));

% Drag Forces
Db=(.5*row*Ab*Cdb).*(V.^2);
Dr=(.5*row*Ar*Cdr).*(V.^2);
```

```
time=x./V;

totaltime(1)=0;
for j=2:(nnz(L)+1)
    totaltime(j)=sum(time(1:j-1))/60;
end

exptime(1)=0;
for j=2:7
    exptime(j)=sum(time(1:j-1))/60;
end

figure
plot(L,totaltime)
title('Buoy Time Response','FontSize',14)
xlabel('Distance from Release Point (m)','FontSize',12)
ylabel('Time (min)','FontSize',12)
grid on
%xlim([0 6])
xlim([0 425])

figure
plot(Vest,Re)
title('Reynolds Number vs. Buoy Velocity','FontSize',14)
xlabel('Velocity of Buoy (m/s)','FontSize',12)
ylabel('Re','FontSize',12)
grid on
xlim([.2 4])
```

8.4 - Hand Calculations

Hand Calculations

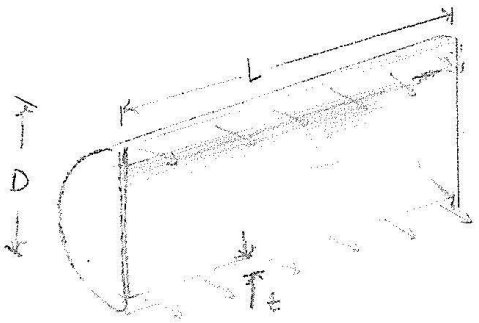

Section View of Housing Vessel

$D = 6.25$ in
$t = 0.375$ in
$L = 10.85$ in

Al Alloy 661
$E = 10007603.9$ psi
$\nu = 0.33$
$\sigma_y = 7998.61$ psi

Internal Pressure: Atmospheric (14.7 psi)

External: 1000 ft submerged (459.1 psi)

Difference: 444.3 psi

Check Buckling

$$\frac{t_{crit}}{D} = \frac{1}{2}\left(1 - \sqrt{\frac{2 \cdot P}{\sigma_{yield}}}\right)$$

$$t_{crit} = \frac{1}{2}\left(1 - \sqrt{\frac{2(444.3\ psi)}{7998.61\ psi}}\right)(6.25\ in) = 0.1848 \text{ inches}$$

0.375 in > 0.1848 in, will not buckle

Longitudinal Stress

$$\sigma_L = \frac{Pr}{2t} = \frac{(-444.3\ psi)(3.125\ in)}{2(0.375\ in)}$$

$\sigma_L = -1851.25$ psi
or 1851.25 compressive

Hoop Stress

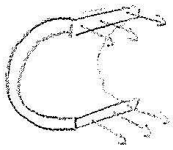

$$\sigma_H = \frac{Pr}{t} = \frac{(-444.3\ psi)(3.125\ in)}{(0.375\ in)}$$

$\sigma_H = -3702.5$ psi
or 3702.5 psi compressive